Biol. Cybern. 86, 457–471 (2002)
DOI 10.1007/s00422-002-0310-9

Biological Cybernetics

Unified neurophysical model of EEG spectra and evoked potentials

C. J. Rennie[1,2], **P. A. Robinson**[1], **J. J. Wright**[3]

[1] School of Physics, University of Sydney, New South Wales 2006, Australia
[2] Department of Medical Physics, Westmead Hospital, Westmead, New South Wales 2145, Australia
[3] Mental Health Research Institute, Parkville, Victoria 3052, Australia

Received: 22 May 2001 / Accepted in revised form: 8 January 2002

Abstract. Evoked potentials – the brain's transient electrical responses to discrete stimuli – are modeled as impulse responses using a continuum model of brain electrical activity. Previous models of ongoing brain activity are refined by adding an improved model of thalamic connectivity and modulation, and by allowing for two populations of excitatory cortical neurons distinguished by their axonal ranges. Evoked potentials are shown to be modelable as an impulse response that is a sum of component responses. The component occurring about 100 ms poststimulus is attributed to sensory activation, and this, together with positive and negative feedback pathways between the cortex and thalamus, results in subsequent peaks and troughs that semiquantitatively reproduce those of observed evoked potentials. Modulation of the strengths of positive and negative feedback, in ways consistent with psychological theories of attentional focus, results in distinct responses resembling those seen in experiments involving attentional changes. The modeled impulse responses reproduce key features of typical experimental evoked response potentials: timing, relative amplitude, and number of peaks. The same model, with further modulation of feedback, also reproduces experimental spectra. Together, these results mean that a broad range of ongoing and transient electrocortical activity can be understood within a common framework, which is parameterized by values that are directly related to physiological and anatomical quantities.

1 Introduction

Evoked response potentials are transient electrical responses to sensory stimuli that can be recorded from the scalp or from within the brain itself. The biophysical mechanism for their generation is thought to be the same as that of the ongoing electroencephalogram (EEG), that is, caused by the extracellular currents induced by neuronal activity. Evoked potentials consist of 'early' components (20–60 ms after the stimulus) that can be ascribed to initial processing of the stimulus, but their most prominent components are the so-called late evoked response potentials (ERPs), which begin about 100 ms after the onset of any stimulus, have the appearance of a damped oscillatory waveform lasting $\approx$200 ms, and resemble EEGs in amplitude ($\approx$10 μV) and frequency content ($\approx$1–20 Hz). Moreover, ERPs are systematically modulated by the tonic level of attention, arousal, cognitive strategy, and by certain mental disorders, and so are a useful objective tool in psychology and psychiatry (Regan 1989).

Figure 1a is the spectrum of an ongoing EEG, and shows a prominent alpha ($\approx$10 Hz) peak, typical of nonfocal cortical activation, such as when the subject is relaxed and not attending to external stimuli. Figure 1b illustrates typical ERPs and the extent of their modulation when experimental conditions are manipulated. In this case a pseudorandom sequence of frequent low tones and infrequent high tones are presented, and the average ERPs corresponding to each are seen to be strong functions of pitch probability. This differentiation requires attention being paid to the pitch differences, and identification of the infrequent and task-relevant tones. Experimental details of the data in Fig. 1 are described elsewhere (Bahramali et al. 1999).

Correlations like this between ERPs and behavioral measures of brain function are easily demonstrated and robust, but tend to lack sensitivity and specificity so that diagnosis and appropriate treatment of patients cannot be inferred from ERPs alone. Yet if their physiological origin were better understood, inverse modeling could be used to infer values for physiological parameters, and thereby enhance the diagnostic value of EEGs and ERPs. Recently we have used this approach to help understand ongoing EEG activity (Rennie et al. 1999; Robinson et al. 1997, 1998; Wright 1999; Wright and Liley 1994), using a continuum approximation of the cortex that included both excitatory and inhibitory

Correspondence to: C. J. Rennie
(e-mail: rennie@physics.usyd.edu.au)

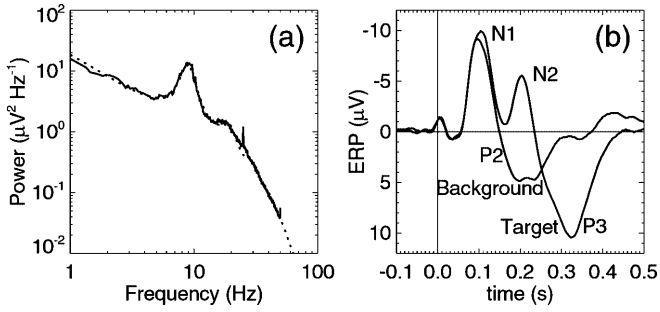

Fig. 1a,b. Typical example of EEG spectrum and evoked response potentials (ERPs) obtained from a group of 40 subjects. **a** EEG spectral power density for subjects who were relaxed with eyes closed: experimental spectrum shown as *solid lines*, fitted spectrum (described below) shown as *dotted lines*. **b** Auditory ERPs in response to frequent, irrelevant ('*background*') tones, and to rare, higher-pitched ('*target*') tones, which are interspersed among the frequent tones. Times are with respect to the stimulus onset, and the peaks are labeled according to the convention for auditory ERPs. Typically '*N*1', '*P*2', '*N*2', and '*P*3' extrema occur respectively at 100 ms, 160 ms, 210 ms, and 320 ms after the stimulus

neural populations, range-dependent connectivities, dendritic delays, and a nonlinear response function. Subsequently this was generalized by the addition of feedback between cortex and thalamus (Robinson et al. 2001b), and was able to relate typical neuronal parameters to overall spectral shape (distinct power-law dependences in different frequency ranges) and to peaks in EEG spectra (forming an approximately harmonic series). The match between the model and observations was demonstrated both for states dominated by *alpha rhythm* (~8–12 Hz) and for sleep spectra characterized by *delta* and *theta rhythms* (1–8 Hz) and by *sleep spindles* (~14 Hz) (Robinson et al. 2001b). We use this model as the starting point for the present model for ERPs.

Of other models of large-scale *collective* neuronal behavior, one of the earliest that mentions ERPs was by Wilson and Cowan (1973), who first introduced the two-dimensional (2-D) continuum approximation for the cortex, reasoning that at scales greater than a few millimeters it should be possible to base a model exclusively on average neuronal properties. At the same time Lopes da Silva et al. (1974) proposed a lumped-parameter thalamocortical model for alpha rhythm. A 2-D continuum model by Nunez (1974, 1995) emphasized the role of long-range excitatory corticocortical connections in large-scale EEG phenomena, perhaps leading to standing waves at the alpha frequency. Elements of these models were combined by Jansen and coworkers in order to model the alpha component of EEGs and visual ERPs (Jansen and Rit 1995; Jansen et al. 1993). There is broad compatibility between all these models regarding the general manner in which to represent neural masses: the differences lie in the chosen anatomical simplifications and the specific phenomena being modeled.

However, a model that addresses the broad range of EEG and ERP phenomena would be of value. As a step towards that end, the current paper describes the extension of our EEG spectral model to the simulation of ERPs. The modifications include more faithful representation of the thalamus and cortex, and the introduction of impulse-like events as precursors of ERPs, as suggested by Wright et al. (1990) based on inverse filtering of experimental data.

Our physiologically based approach contrasts – particularly regarding the choice of parameters – with phenomenological models that are often used for quantifying ERPs; e.g., using band-pass filtering (Robinson 1999), factor decomposition (Makeig et al. 1999), superpositions of damped sine waves (Shibasaki et al. 1987), and wavelets (Samar et al. 1995).

The main characteristics of ERPs that we address are the relative timing and amplitudes of several peaks in ERPs, particularly those evoked in response to trains of discrete stimuli (of any sensory modality) where there are two randomly interspersed variations of the stimulus – the so-called oddball paradigm – as shown in Fig. 1b. The characteristics that we aim to reproduce are (i) response onsets that are appropriately delayed with respect to the stimuli, (ii) a damped oscillatory response, (iii) an approximately 4-Hz dominant frequency, and (iv) the occurrence (typically observed following simple stimuli) of negative and positive extrema of similar magnitude, that are *not* followed by additional extrema. Moreover this should be done in a way that retains the ability to reproduce the ongoing EEG spectrum without any alteration to the model – apart from the form of the driving signal, and parameter modulations that are physiologically plausible.

Section 2 describes the extended model, including expressions for the frequency- and time-domain characteristics of the system. The general characteristics of the modeled spectra and evoked potentials are demonstrated in Sect. 3. The spectral equations, which are generalized in several ways from our previous work, are shown to remain compatible with observations. Various predictions of the ERP equations are then explored, using parameters that are consistent with the EEG spectra. The results are discussed in Sect. 4.

2 Model

This section summarizes the basic model for collective neuronal dynamics developed in our previous work, and extends it to represent the cortex and thalamus in more detail. The intention is to derive a model of the large-scale dynamics of the EEG; and so we employ simplifications that are extreme when compared with some other models, but are expected to be valid in the linear limit and for a large-enough ensemble of neurons.

In the linear limit and for randomly interconnected excitatory and inhibitory neurons, a model for an unbounded homogeneous cortex can be derived with the transfer function (Robinson et al. 2001b)

$$\frac{\phi_{\rm e}(\boldsymbol{k},\omega)}{\phi_{\rm s}(\boldsymbol{k},\omega)} = \frac{G_{\rm es}L(\omega)}{D_{\rm e}(\boldsymbol{k},\omega)[1-G_{\rm ii}L(\omega)]-G_{\rm ee}L(\omega)} \quad . \tag{1}$$

The function $\phi_{\rm e}(\boldsymbol{r},t)$ is the rate of action potentials arriving at a point $\boldsymbol{r}$ from excitatory neurons elsewhere

in the cortex, and $\phi_s(\boldsymbol{r},t)$ is the activity from subcortical neurons.

The remaining functions appearing in (1) are

$$L(\omega) = (1 - i\omega/\alpha)^{-1}(1 - i\omega/\beta)^{-1} \ , \tag{2}$$

which approximates the low-pass response of the dendritic portion of each neuron [in the time domain the impulse response is $\alpha\beta(e^{-\alpha\tau} - e^{-\beta\tau})/(\beta - \alpha)$ for $\tau \geq 0$], and

$$D_e(\boldsymbol{k},\omega) = k^2 r_e^2 + (1 - i\omega/\gamma_e)^2 \ , \tag{3}$$

which is obtained from the 2-D damped wave equation that we use to approximate the spread of activity through the cortex (r_e is the characteristic length for excitatory axons and $\gamma_e = v/r_e$ is the characteristic damping rate assuming a uniform speed v of action potentials along axons). In deriving (1) it was assumed that inhibitory axon lengths were short compared with the scale of EEGs, with the result that the inhibitory analog of (3) is $D_i(\boldsymbol{k},\omega) = 1$. The transfer function describing the firing rate at inhibitory synapses is closely related to (1):

$$\frac{\phi_i(\boldsymbol{k},\omega)}{\phi_s(\boldsymbol{k},\omega)} = \frac{G_{is}D_e}{G_{es}}\frac{\phi_e}{\phi_s} \ . \tag{4}$$

Equations (1) and (4) can be written in terms of more fundamental neuronal parameters, including the average number N_{ab} of synapses from neurons of type b = e,i,s on neurons of type a = e,i; the sizes s_b of postsynaptic potentials; and the shape of the sigmoidal relationship between membrane depolarization V_a and firing rate Q_a. [The subscripts refer to excitatory (e), inhibitory (i), and subcortical (s) neural populations.] However, these quantities are more conveniently combined into the dimensionless gains $G_{ab} = \rho_a N_{ab} s_b$, where $\rho_a = dQ_a/dV_a$ is the derivative of the assumed sigmoidal response function,

$$Q_a = \frac{Q_a^{\max}}{1 + \exp[-(\pi/\sqrt{3})(V_a - \theta_a)/\sigma_a]} \ , \tag{5}$$

evaluated at the steady state of the system (Robinson et al. 1997). Note that the common factors in the expressions for the six gains G_{ab} mean that they are not independent. Moreover, we assume that the number of interconnections between neuronal types is proportional to the number of available synapses, so the six values N_{ab} are interdependent. The existence of these implicit interrelations among the gains are the reason that only three appear explicitly in (1).

To make use of (1), some form must be given to the quantity $\phi_s(\boldsymbol{k},\omega)$. The signal reaching the cortex from subcortical gray matter is known to be a mixture of sensory signals and feedback activity. The latter involves pathways from the cortex, via the basal ganglia, thalamus, or hippocampal formation, and back to the cortex. Rather than attempt to represent the considerable complexity of these pathways in a functional form, we shall adopt a simple form for ϕ_s, consisting of a single sensory source and one feedback loop between thalamus and cortex, and generalize to multiple loops later, if necessary. The details of this simplification follow.

2.1 Thalamic model

The thalamus consists of roughly 15 relay nuclei, within which are excitatory neurons that either relay sensory signals to specific areas of the cortex (primary relay circuits) or feed cortical activity back to the cortex (secondary relay circuits). The latter project with various specificity to the cortex, and can be loosely divided into 'specific' and 'nonspecific' nuclei. In addition there is the *reticular nucleus of the thalamus* and the *perigeniculate nucleus*, which envelop and project inhibitory connections to the relay nuclei, as well as receiving excitatory collaterals from the interconnections between relay nuclei and the cortex. [For brevity in what follows we shall refer only to the thalamic reticular nucleus (TRN) and to thalamic relay nuclei collectively.] Considerable interest surrounds the TRN, as its structure and connections gives it the potential to influence activity throughout the thalamus, and so is believed to have an important role in the gating of cortical inputs during sleep and arousal, and in effecting focal attention. The former relies on general inhibition of the relay nuclei to gate sensory activity reaching the cortex (Yingling and Skinner 1977), while the latter proposal – known as the 'searchlight hypothesis' – presumes there to be some mechanism mediated by the TRN by which one portion of the thalamocortical connections is selected, while the remaining parts are inhibited (Crick 1984). Subsequent investigations have identified possible physiological mechanisms postulated by the searchlight hypothesis, but difficulties in interpreting the evidence have prevented identification of which, if any, result in attentional focus. Others have emphasized the role of the feedback loop between cortex and thalamus, where '...the cortical influence can either promote or antagonize the relay of information, depending on the state of the dendrites of the reticular neurons' (Destexhe 2000).

This paper will adopt the general idea that information processing is facilitated by transient modulations in the operating characteristics of the thalamus, which can be represented by varying thalamic gains. We shall consider later the origin of the presumed gain modulations, although we note now the existence of modulatory inputs to the thalamus mediated by acetylcholine and biogenic amines, and that there is evidence that the reticular nucleus is modulated in this way during the generation of ERPs (Steriade et al. 1990; Swick et al. 1994).

Figure 2 depicts the relationship between cortex, reticular nucleus, and a typical specific or secondary relay nucleus. Also shown are the transmission delays inherent in corticothalamic fibers and various gains G_{ab} defined similarly to cortical gains as the ratio of firing rate changes in target and source neural populations, where the changes are with respect to the steady state values. The reticular nucleus is unlike all other thalamic nuclei in that (i) it receives input from all relay nuclei (different

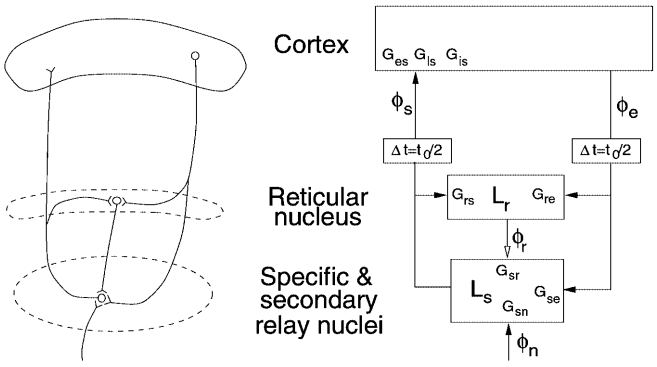

Fig. 2. Connections within the thalamus, and between the thalamus and cortex: anatomical (*left*) and schematic (*right*). In the schematic diagram, *filled arrows* represent excitatory connections and *open arrows* represent inhibitory connections. The G_{ab} are gains operating on firing rates ϕ_e, ϕ_n, and ϕ_r. The transfer functions of the reticular nucleus and the specific or secondary relay nuclei are $L_r(\omega)$, and $L_s(\omega)$, respectively

relay nuclei are not directly interconnected), and (ii) its neurons are inhibitory in function (whereas the majority of relay neurons are excitatory). Note that on the basis of known physiology all gains shown are expected to be positive except for G_{sr}, which is negative due to the inhibition of specific and secondary relay nuclei by the reticular nucleus.

We assume here that feedback between cortex and thalamus approximately preserves spatial relationships. This is indeed the case for *specific* relay nuclei (e.g., those reciprocally connected with primary sensory cortex), but less true for *secondary* relay nuclei (e.g., those connected with association cortex), which can receive convergent activity from the cortex and project divergently to the cortex, thereby filtering out larger wave numbers. In order to model this blurring in the thalamocortical pathways conveniently, we shall permit the driving signal ϕ_n to be spatially nonwhite, although we shall assume it to be temporally white, in common with previous work. Accordingly we find that $\phi_s(\boldsymbol{k},\omega)$ is given by

$$\phi_s = \mathscr{P}\phi_n + \mathscr{S}\phi_e \ , \tag{6}$$

where $\mathscr{P}$ is the thalamocortical transfer function and $\mathscr{S}$ is the corticothalamocortical transfer function, and

$$\mathscr{P}(\omega) = \frac{L_s G_{sn}}{1 - L_s G_{sr} L_r G_{rs}} e^{i\omega t_0/2} \ , \tag{7}$$

$$\mathscr{S}(\omega) = \frac{L_s G_{se} + L_s G_{sr} L_r G_{re}}{1 - L_s G_{sr} L_r G_{rs}} e^{i\omega t_0} \ . \tag{8}$$

Equation (6) assumes the noise to arise at or below the level of the thalamus. However, alternative sources might be postulated for the driving signal ϕ_n; e.g., the noise might be intrinsic to the cortex, or else it might arise in some cortical region and reach other cortical regions via the thalamus. These options can be accommodated in (6) by replacing the thalamocortical transfer function $\mathscr{P}$ by 1 or by $\mathscr{S}$, respectively.

2.2 Cortical model

The linear damped wave equation used by us to represent the spread of activity through the cortex corresponds to a distribution of axon ranges proportional to the modified Bessel function of the second kind, $K_0(|\boldsymbol{r}|/r_e)$ (Robinson et al. 1997). This function is monotonic decreasing with an integrable singularity at the origin, and has been used to approximate the axonal range distribution of excitatory neurons. However, given that the majority of excitatory neurons are thought to have connections limited to the minicolumn in which they reside, it can be argued that the proportion of short-range connections may be even greater than implied by the Bessel function distribution. To accommodate this we should include a second excitatory population to our model, which can be described in the same way as the first, but with axonal ranges $\sim$0.1 mm; i.e., much less than both r_e and the typical spacing of electrodes. This generalization is important when later modeling ERPs, and we discuss the likely relative contributions of the two populations in Sect. 3.

If we indicate the additional population with the subscript l, then the field equations are

$$D_e\phi_e = L_e G_{ee}\phi_e + L_e G_{el}\phi_l + L_e G_{ei}\phi_i + L_e G_{es}\phi_s \ , \tag{9}$$

$$D_l\phi_l = L_l G_{le}\phi_e + L_l G_{ll}\phi_l + L_l G_{li}\phi_i + L_l G_{ls}\phi_s \ , \tag{10}$$

$$D_i\phi_i = L_i G_{ie}\phi_e + L_i G_{il}\phi_l + L_i G_{ii}\phi_i + L_i G_{is}\phi_s \ , \tag{11}$$

which describe the dendritic summation and the cortical propagation of the resultant activity for each of the three classes of neurons.

With the help of (6), (9)–(11) can be written as

$$\begin{bmatrix} D_e - L_e G_{ee} - L_e G_{es}\mathscr{S} & -L_e G_{el} & -L_e G_{ei} \\ -L_l G_{le} - L_l G_{ls}\mathscr{S} & D_l - L_l G_{ll} & -L_l G_{li} \\ -L_i G_{ie} - L_i G_{is}\mathscr{S} & -L_i G_{il} & D_i - L_i G_{ii} \end{bmatrix} \begin{bmatrix} \phi_e \\ \phi_l \\ \phi_i \end{bmatrix} = \begin{bmatrix} L_e G_{es} \\ L_l G_{ls} \\ L_i G_{is} \end{bmatrix} \mathscr{P}\phi_n \ . \tag{12}$$

After solving for ϕ_e, ϕ_l, and ϕ_i we then find

$$\begin{bmatrix} \phi_e \\ \phi_l \\ \phi_i \end{bmatrix} = \frac{1}{\det} \left(\begin{bmatrix} D_l D_i & D_i L_e G_{el} & D_l L_e G_{ei} \\ D_i(L_l G_{le} + L_l G_{ls}\mathscr{S}) & D_i D_e & D_e L_l G_{li} \\ D_l(L_i G_{ie} + L_i G_{is}\mathscr{S}) & D_e L_i G_{il} & D_e D_l \end{bmatrix} - \operatorname{diag} \begin{bmatrix} D_l L_i G_{ii} + D_i L_l G_{ll} \\ D_i L_e(G_{ee} + G_{es}\mathscr{S}) + D_e L_i G_{ii} \\ D_e L_l G_{ll} + D_l L_e(G_{ee} + G_{es}\mathscr{S}) \end{bmatrix} \right) \times \begin{bmatrix} L_e G_{es} \\ L_l G_{ls} \\ L_i G_{is} \end{bmatrix} \mathscr{P}\phi_n \ , \tag{13}$$

where

$$\det = D_e D_l D_i - (L_e G_{ee} + L_e G_{es}\mathscr{S}) D_l D_i - D_e L_l G_{ll} D_i - D_e D_l L_i G_{ii} \ , \quad (14)$$

and diag denotes a diagonal matrix with the elements shown. Hence,

$$\frac{\phi_e}{\phi_n} = D_l D_i L_e G_{es}\mathscr{P}/\det \ , \quad (15)$$

$$\frac{\phi_l}{\phi_n} = D_e D_i L_l G_{ls}\mathscr{P}/\det \ , \quad (16)$$

$$\frac{\phi_i}{\phi_n} = D_e D_l L_i G_{is}\mathscr{P}/\det \ . \quad (17)$$

These results use simplifications that follow from the random connectivity assumption for cortical neurons: specifically the symmetries $G_{ab}G_{cd} = G_{ad}G_{cb}$, where $a, c =$ e,l,i and $b, d =$ e,l,i,s (Robinson et al. 1997).

From the above equations it can be shown that

$$\frac{\phi_e}{\phi_n} = \frac{\lambda L_e G_{es}\mathscr{P}}{k^2 r_e^2 + q^2 r_e^2} M \ , \quad (18)$$

where

$$\lambda = \frac{1}{1 - L_l G_{ll} - L_i G_{ii}} \ , \quad (19)$$

$$q^2 r_e^2 = (1 - i\omega/\gamma_e)^2 - \lambda L_e G_{ee} - \lambda L_e G_{es}\mathscr{S} \ , \quad (20)$$

$$M = 1 + \frac{D_e L_l G_{ll} D_i (1 - D_l) + D_e D_l L_i G_{ii} (1 - D_i)}{\det} \ . \quad (21)$$

We note also that the axon lengths r_l and r_i are sufficiently small that $D_a = k^2 r_a^2 + (1 - i\omega/\gamma_a)^2 \approx 1$ for $a =$ l,i. The reason is that wavenumbers are limited to $k_{max} \lesssim 2\pi/r_e$ by the wide reach of population e axons, and frequencies are limited to $\omega_{max} \sim \alpha$ by dendritic filtering, so that $k_{max} r_a \sim 2\pi r_a/r_e \ll 1$, and similarly $\omega_{max}/\gamma_a \sim 2\pi\alpha r_a/v \ll 1$. As a result of $D_l \approx D_i \approx 1$, $M \approx 1$ and (18) becomes identical to the corresponding expression used in earlier work, other than replacement throughout of $L_i G_{ii}$ by $L_l G_{ll} + L_i G_{ii}$. The newly introduced excitatory population (with subscript l) affects ϕ_e/ϕ_n only insofar as predictions now depend on this lumped measure of the two short-axon populations. If the dendritic time constants of the two populations are similar, so that $L_l \approx L_i$, then inverse modeling from real data will not be able to estimate G_{ll} and G_{ii} separately.

The form of the response in short-axon excitatory neurons $\phi_l(\boldsymbol{k}, \omega)$ is best viewed in relation to $\phi_e(\boldsymbol{k}, \omega)$. If we take (15) and (16), we find

$$\frac{\phi_l}{\phi_n} = \frac{D_e L_l G_{ls}}{D_l L_e G_{es}} \frac{\phi_e}{\phi_n} \ . \quad (22)$$

Then

$$\frac{\phi_l}{\phi_n} = \lambda L_l G_{ls}\mathscr{P} \frac{M}{D_l} \frac{k^2 r_e^2 + (1 - i\omega/\gamma_e)^2}{k^2 r_e^2 + q^2 r_e^2} \ , \quad (23)$$

$$= \lambda L_l G_{ls}\mathscr{P} \frac{M}{D_l} \left[1 + \frac{\lambda L_e G_{ee} + \lambda L_e G_{es}\mathscr{S}}{k^2 r_e^2 + q^2 r_e^2}\right] \ , \quad (24)$$

so,

$$\phi_l = \lambda L_l G_{ls}\mathscr{P} \frac{M}{D_l} \phi_n + \frac{\lambda L_l G_{ls}}{L_e G_{es} D_l} (L_e G_{ee} + L_e G_{es}\mathscr{S}) \phi_e \ , \quad (25)$$

$$= \lambda L_l G_{ls}\mathscr{P} \frac{M}{D_l} \phi_n + \frac{\lambda L_l G_{le}}{D_l} \phi_e + \frac{\lambda L_l G_{ls}\mathscr{S}}{D_l} \phi_e \ . \quad (26)$$

Equation (26) is obtained from the preceding equation by relations implied by the random connectivity assumption (Robinson et al. 1997). The corresponding result for $\phi_i(\boldsymbol{k}, \omega)$ can simply be obtained by exchanging the subscripts l and i. As a result, the remainder of this section will deal only with the e and l populations, and the latter can be thought of as referring either to local excitatory or local inhibitory neurons.

2.3 Spectra

In deriving the expected form of EEG spectra we assume that the scalp potential is proportional to some linear combination of the synaptic firing rates, as discussed below in Sect. 3.1. Hence $|V(\omega)|^2 = |w_e\phi_e + w_l\phi_l + w_i\phi_i|^2$, where the weights w_a depend on many (constant) neuronal and volume conduction factors. Here we shall consider just the two functions, $|\phi_e|^2$ and $|\phi_l|^2$, since $|\phi_i|^2$ can be obtained trivially from $|\phi_l|^2$, the various cross terms are intermediate in character between the two principal cases, and absolute estimates are not needed in the present context.

From (18) and (22),

$$|\phi_e(\boldsymbol{k}, \omega)|^2 = \left|\frac{\lambda L_e G_{es}\mathscr{P}}{k^2 r_e^2 + q^2 r_e^2}\right|^2 |M|^2 |\phi_n|^2 \ , \quad (27)$$

$$|\phi_l(\boldsymbol{k}, \omega)|^2 = \left|\frac{D_e L_l G_{ls}}{D_l L_e G_{es}}\right|^2 |\phi_e|^2 \ . \quad (28)$$

To obtain expressions for the conventional spectral measures $|\phi_e(\omega)|^2$ and $|\phi_l(\omega)|^2$ we commonly assume that ϕ_n is spatially white. However, thalamocortical axons individually and collectively have nonzero spread within the cortex, and so it is more realistic to assume a limit on the range of wavenumbers reaching the cortex. We shall assume

$$|\phi_n(\boldsymbol{k}, \omega)|^2 = (r_s^2/2\pi) \exp(-k^2 r_s^2/2) |\phi_n(\omega)|^2 \ , \quad (29)$$

which limits wavenumbers to $k \lesssim 2\pi/r_s$. The spatial component of $|\phi_n(\boldsymbol{k}, \omega)|$ is the Fourier transform of a 2-D Gaussian distribution with standard deviation r_s, and $|\phi_n(\boldsymbol{k}, \omega)|^2$ satisfies the condition $\int |\phi_n(\boldsymbol{k}, \omega)|^2 d^2\boldsymbol{k} = |\phi_n(\omega)|^2$. Then

$$|\phi_e(\omega)|^2 = |\lambda L_e G_{es}\mathscr{P}|^2 \int \frac{|M|^2|\phi_n(\boldsymbol{k},\omega)|^2}{|k^2r_e^2+q^2r_e^2|^2}\mathrm{d}^2\boldsymbol{k}\ , \tag{30}$$

$$= |\phi_n(\omega)|^2|\lambda L_e G_{es}\mathscr{P}|^2\frac{r_s^2}{2\pi}\int \frac{|M|^2\mathrm{e}^{-k^2r_s^2/2}}{|k^2r_e^2+q^2r_e^2|^2}\mathrm{d}^2\boldsymbol{k}\ ,$$

$$= |\phi_n(\omega)|^2|\lambda L_e G_{es}\mathscr{P}|^2\frac{-\kappa}{\mathrm{Im}\,q^2r_e^2} \tag{31}$$

$$\times\,\mathrm{Im}\left(\mathrm{e}^{q^2r_e^2\kappa}E_1(q^2r_e^2\kappa)\right)\ , \tag{32}$$

where we have introduced $\kappa = r_s^2/2r_e^2$ as the measure of the wavenumber content of the driving signal, and E_1 is an exponential integral (Abramowitz and Stegun 1965). Equation (32) follows from the integrand's effective wave number cutoff $\sim 2\pi/r_e$ and frequency cutoff $\sim\alpha$, for which $|M|^2 \approx 1$. If $r_s \ll r_e$ (the driving signal is spatially nearly white) then (32) simplifies to

$$|\phi_e(\omega)|^2 = |\phi_n(\omega)|^2|\lambda L_e G_{es}\mathscr{P}|^2\kappa\frac{\arg q^2r_e^2}{\mathrm{Im}\,q^2r_e^2}\ . \tag{33}$$

The equivalent expression for ϕ_l is

$$|\phi_l(\omega)|^2 = \left|\frac{L_l G_{ls}}{L_e G_{es}}\right|^2|\lambda L_e G_{es}\mathscr{P}|^2$$

$$\times\int\frac{|D_e|^2}{|D_l|^2}\frac{|M|^2|\phi_n(\boldsymbol{k},\omega)|^2}{|k^2r_e^2+q^2r_e^2|^2}\mathrm{d}^2\boldsymbol{k}\ . \tag{34}$$

In this case the presence of $D_e = k^2r_e^2 + (1-\mathrm{i}\omega/\gamma_e)^2$ in the numerator means that the integrand is not low-pass limited to $k \lesssim 2\pi/r_e$ as in (32). Instead the integrand has an effective high-frequency cutoff in wave number due to the Gaussian envelope of the noise function, and in frequency due to the dendritic filter functions L_a. Provided the spatial and temporal frequencies are limited to $\ll 2\pi/r_{l,i}$ and $\ll v/r_{l,i}$, respectively, then both $|D_l|^2$ and $|M|^2 \approx 1$, and thus

$$|\phi_l(\omega)|^2 = |\phi_n(\omega)|^2|\lambda L_l G_{ls}\mathscr{P}|^2\frac{r_s^2}{2\pi}$$

$$\times\int\frac{|k^2r_e^2+(1-\mathrm{i}\omega/\gamma_e)^2|^2}{|k^2r_e^2+q^2r_e^2|^2}\mathrm{e}^{-k^2r_s^2/2}\mathrm{d}^2\boldsymbol{k}\ ,$$

$$= |\phi_n(\omega)|^2|\lambda L_l G_{ls}\mathscr{P}|^2$$

$$\times\left[1-\frac{\kappa}{\mathrm{Im}\,q^2r_e^2}\mathrm{Im}\left(q^4r_e^4\mathrm{e}^{q^2r_e^2\kappa}E_1(q^2r_e^2\kappa)\right)\right.$$

$$+\frac{2(1-\omega^2/\gamma_e^2)\kappa}{\mathrm{Im}\,q^2r_e^2}\mathrm{Im}\left(q^2r_e^2\mathrm{e}^{q^2r_e^2\kappa}E_1(q^2r_e^2\kappa)\right)$$

$$\left.-\frac{(1+\omega^2/\gamma_e^2)^2\kappa}{\mathrm{Im}\,q^2r_e^2}\mathrm{Im}\left(\mathrm{e}^{q^2r_e^2\kappa}E_1(q^2r_e^2\kappa)\right)\right]\ . \tag{35}$$

The corresponding expression for $|\phi_i(\omega)|^2$ can be obtained by exchanging the subscripts l and i.

2.4 Evoked response potentials

For the purposes of modeling ERPs we shall take the same model as was discussed in the context of spectra, and replace incoming white noise with an impulsive stimulus. The driving signal will be taken as a pulse of limited spatiotemporal extent,

$$\phi_n(\boldsymbol{k},\omega) = \mathrm{e}^{-k^2r_s^2/4}\mathrm{e}^{-\omega^2t_s^2/2}\ , \tag{36}$$

which is normalized in coordinate space to have unit integral and standard deviations of r_s spatially and t_s temporally. This expression has the advantage of being more general and realistic than δ-function alternatives. The spatial component of ϕ_n means that the impulse produces a cortical activation that has the form of a 2-D Gaussian, the extent of which (r_s) is really a property of the divergent sensory thalamocortical pathways, but it is convenient to lump it with the temporal distribution of the driving signal. In the derivations that follow, t_s will be assumed to be $\sim$10 ms and of the same order as $1/\alpha$, $1/\beta$, and $1/\gamma_e$, but much greater than $1/\gamma_l$ or $1/\gamma_i$. The appropriate spatial extent r_s of the stimulus is less definite, but is plausibly >10 mm (observed to be the smallest extent of cortex that can be activated by a stimulus) and certainly <500 mm (the circumference of the brain). These bounds on allowed wavenumbers and frequencies permit the approximations $M \approx D_l \approx 1$ to be made below.

With the above assumptions, the response $\phi_e(R,t)$ at some distance R from the center of the impulse is

$$\phi_e(R,t) = \int_0^\infty \mathrm{d}k\frac{k}{2\pi}J_0(kR)$$

$$\times\,\mathscr{F}^{-1}\left\{\frac{\phi_e}{\phi_n}\mathrm{e}^{-k^2r_s^2/4}\mathrm{e}^{-\omega^2t_s^2/2}\right\}\ , \tag{37}$$

$$\approx \int_0^\infty \mathrm{d}k\frac{k}{2\pi}J_0(kR)$$

$$\times\,\mathscr{F}^{-1}\left\{\lambda L_e G_{es}\mathscr{P}\frac{\mathrm{e}^{-k^2r_s^2/4}\mathrm{e}^{-\omega^2t_s^2/2}}{k^2r_e^2+q^2r_e^2}\right\}\ , \tag{38}$$

where $\mathscr{F}^{-1}$ represents the inverse temporal Fourier transform, and $M \approx D_l \approx 1$ is assumed.

For the same stimulus, $\phi_l(\boldsymbol{k},\omega)$ is

$$\phi_l(\boldsymbol{k},\omega) = \frac{D_e L_l G_{ls}}{D_l L_e G_{es}}\frac{\phi_e}{\phi_n}\mathrm{e}^{-k^2r_s^2/4}\mathrm{e}^{-\omega^2t_s^2/2}\ , \tag{39}$$

and like (26) this can be written as the sum of three terms, the latter two of which are closely related to ϕ_e:

$$\phi_l(\boldsymbol{k},\omega) = \lambda L_l G_{ls}\mathscr{P}\frac{M}{D_l}\mathrm{e}^{-\frac{k^2r_s^2}{4}}\mathrm{e}^{-\frac{\omega^2t_s^2}{2}}$$

$$+\frac{\lambda L_l G_{le}}{D_l}\phi_e + \frac{\lambda L_l G_{ls}\mathscr{S}}{D_l}\phi_e\ . \tag{40}$$

The three terms in (40) have different spatial and temporal characteristics, which we shall consider in

turn. Assuming, for reasons given above, that $M = D_l = 1$, the first term can be spatially inverse transformed giving

$$\frac{1}{\pi r_s^2} e^{-R^2/r_s^2} \mathscr{F}^{-1}\left\{\lambda L_l G_{ls} \mathscr{P} e^{-\omega^2 t_s^2/2}\right\} . \quad (41)$$

This term is limited spatially to $R \lesssim r_s$, and has no terms relating to long-axon neurons. Physically, it is the initial response of short-axon neurons to subcortical activation.

The second term in (40) is the component of ϕ_l that is due to direct driving by ϕ_e. The factor $L_l G_{le}$ describes the filtering and gain experienced by a signal passing through a local neuron; the factor $\lambda = 1/(1 - L_l G_{ll} - L_i G_{ii})$ describes the modulation of ϕ_e by the short-range neural populations, and is of a form that is commonly encountered in systems where there is additive filtered feedback. Only corticocortical connections are involved in this term. The presence of the term L_l means that a delay of order $1/\alpha + 1/\beta$ with respect to ϕ_e can be expected.

The last term in (40) can also be considered to be due to ϕ_e, but in this case includes $\mathscr{S}$, equal to the corticothalamic transfer function ϕ_s/ϕ_e. Consequently this term describes feedback of ϕ_e from the cortex, through the corticothalamic loop, to short-axon neurons in the cortex. There is a delay of order $1/\alpha + 1/\beta$, as with the preceding term, but there is an additional delay t_0 due to the finite conduction speed in the corticothalamic loop (see Eq. 8), as well as the delay within the thalamus.

3 Characteristics of the model

This section compares the theory of Sect. 2 with experimental data. In order to obtain representative parameter values for numerical examples in this section, (33) was first fitted to the experimental spectrum shown in Fig. 1a, which yielded the values listed in Table 1. Note that in general the equations allow only certain compound gains to be inferred: $G_{es}G_{se}$ is the net gain of the direct corticothalamic feedback; $G_{es}G_{sr}G_{re}$ is the net corticothalamic feedback via the TRN; and $G_{sr}G_{rs}$ is the net gain between the relay nuclei and TRN.

3.1 Spectra

We have discussed fitting of an earlier version of the model to experimental spectra elsewhere (Robinson et al. 2001b), so here we shall cover only the variations due to the additional features of the current version of the model. They include (i) the site of the noise generator, (ii) the effect of spatial filtering of subcortical feedback, (iii) resonances internal to the thalamus, and (iv) the relative contributions of ϕ_e, ϕ_l, and ϕ_i to spectra recorded from the scalp.

It was noted in connection with (6) that the generator of noise might be hypothesized to lie in various parts of the brain, and that the principal alternatives to the version in Fig. 2 could both be accommodated by suitable redefinition of $\mathscr{P}$. Anatomically the choice is unclear, since the reticular activating system provides a continuous driving signal to both the thalamus and cortex; but at the same time there is spontaneous firing within the cortex which could also be seen as a driving signal. Mathematically, the consequences of these alternatives are simply understood since the spectral expressions (32) and (35) are proportional to $|\mathscr{P}(\omega)|^2$. When $\mathscr{P}$ is defined by (7), corresponding to noise entering at the thalamus, its magnitude is asymptotically proportional to ω^{-2}, as is the case when $\mathscr{P} \to \mathscr{S}$ (white noise arriving at the cortex via the corticothalamic pathway from elsewhere in the cortex), and in contrast to the case when $\mathscr{P} \to 1$ (noise arriving unfiltered at the cortex). Given sufficiently noise-free data it should be possible to identify which of the three possibilities best resembles experimental data through their different cutoff characteristics and asymptotic behavior. However, the parameters α, β, γ_e, η_1, and η_2 all also influence the spectral shape, and we find in practice that the noisy experimental spectrum in Fig. 1a can be equally well fitted with all three source alternatives, when suitable adjustments are made to the rate constants. Furthermore, independent estimates of the five rate constants have uncertainty factors of $\sim$2, and the critical high-frequency asymptote is obscured by biological and instrumental noise, and so none of the three alternatives can be confidently eliminated at present. Table 1 was derived by assuming $\mathscr{P}$ to be given by (7), corresponding to a noise source projecting to the thalamus.

The second of the issues listed above – the effect of spatial filtering – arose in Sect. 2.3 from the desire to employ a thalamocortical signal with a realistic spatial spectrum. Limiting of the spatial frequency content of this signal could be intrinsic to the noise source or be imposed by convergence and divergence within the corticothalamic feedback loops discussed in Sect. 2.1. The contribution of the different wave numbers has been

Table 1. Parameters values obtained by fitting (33) to an EEG spectrum obtained from averaging the spectra from 40 normal subjects (total of 40×2 minutes recorded from vertex of the head). The method for fitting is described elsewhere (Robinson et al. 2001b). During the fitting procedure, the value of v was fixed and equal to the value from Nunez (1995) (which, together with γ_e, implies $r_e = 0.08$ m), while others were constrained ($L_e = L_l = L_i$, $\beta/\alpha = \eta_2/\eta_1$) as the theoretical spectrum is relatively insensitive to these parameters

Parameter	Value	Units
γ_e	142	s^{-1}
α	36	s^{-1}
β	730	s^{-1}
η_1	51	s^{-1}
η_2	1000	s^{-1}
$G_{ll} + G_{ii}$	-5.9	
G_{ee}	1.3	
$G_{es}G_{se}$	6.9	
$G_{es}G_{sr}G_{re}$	-0.98	
$G_{sr}G_{rs}$	-0.14	
t_0	0.08	s
v	10	m s^{-1}

examined elsewhere in the context of modal analysis, where it was found that boundary effects are negligible except when strong resonances occur and the waves are very weakly damped (Robinson et al. 2001a). Here we shall look instead at varying the wave number cutoff parameter, r_s. We take the circumference of the brain as an upper limit to the range of wavelengths to consider. As a lower limit, we again use $\sim$10 mm, the smallest cortical extent that can be activated by a stimulus. Taking these values, those in Table 1, and (32) and (35), we can calculate numerical estimates of the expected spectra, as seen in Fig. 3.

The asymptotic behavior and characteristics of the spectral peaks of $|\phi_e|^2$ were discussed by Robinson et al. (2001b) for the spatially white noise case, $r_s \to 0$. In the same limit the constant term in (35) tends to dominate, resulting in a featureless spectrum for $|\phi_e|^2$ described mainly by the term in front of the integral. In the other limit $r_s \to \infty$, corresponding to spatially uniform noise, $|\phi_e|^2$ and $|\phi_l|^2$ differ only by a factor $|1 - i\omega/\gamma_e|^2$, so are similar at frequencies $< \gamma_e \approx 20$ Hz. Other than near peaks, both $|\phi_e|^2$ and $|\phi_l|^2$ are steeper when r_s is large than when $r_s \to 0$. In practice we find that experimental spectra generally resemble $|\phi_e|^2$ for $r_s \approx 0$, but the same spectra might also be due to $|\phi_l|^2$ with an intermediate value of r_s. As such it is difficult to infer the value of r_s from spectral fits alone.

Concerning the third of the issues listed above, it is of interest to note that the thalamocortical transfer function $\mathscr{P}$, which appears in both (32) and (35), has a dispersion relation $1 - L_s G_{sr} L_r G_{rs} = 0$. This yields a fourth-order polynomial that can be solved for ω in terms of the thalamic rate constants and gains G_{sr} (a negative quantity) and G_{rs}. We find

$$\omega = -i\left(\frac{\eta_1 + \eta_2}{2}\right) \pm \sqrt{\left(\frac{\eta_1 - \eta_2}{2}\right)^2 \pm i\eta_1\eta_2\sqrt{|G_{sr}|G_{rs}}}\,, \quad (42)$$

and the two roots that are least damped become linearly unstable at a frequency $\sqrt{\eta_1\eta_2}$ when $|G_{sr}|G_{rs} = (\eta_1 + \eta_2)^2/(\eta_1\eta_2) \sim 10$. The instability is due to undamped feedback between the two elements of the thalamus, and so is unrelated to the corticothalamic resonance responsible for the peaks in Fig. 3. The resonant frequency $\sqrt{\eta_1\eta_2} \approx 135\ s^{-1} \approx 20$ Hz is in the range of practical interest, so is potentially relevant if the intrathalamic gains are sufficiently strong.

A final issue is how the modeled variables ϕ_e, ϕ_l, and ϕ_i relate to the potentials measured on the scalp. Each impulse arriving at a synapse triggers a depolarization or hyperpolarization of the dendritic membrane, which largely attenuates with a time constant $\sim$2 ms (Koch 1999, p. 75). The variables ϕ_e, ϕ_l, and ϕ_i are therefore good proxies for the extracellular currents induced by synaptic action. Also, we take these signals to be approximately proportional to their corresponding scalp potentials, under the assumption that many of complications diminish on large, slow scales typical of EEGs. However, this simplification is contingent upon further investigations in the area of anatomy and modeling of extracellular potentials.

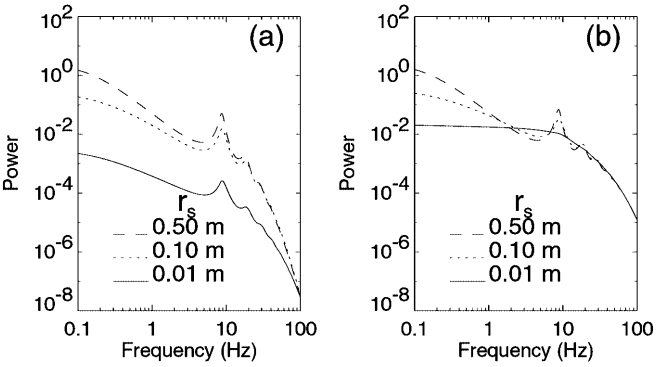

Fig. 3a,b. Modeled spectral power density functions (arbitrary units). Spatial and temporal white noise is assumed, except that the spatial wave numbers of the noise are limited by a Gaussian function $(r_s^2/2\pi)\exp(-k^2r_s^2/2)$. Spectra are shown for three values of r_s, and other parameters are from Table 1. **a** $|\phi_e(\omega)|^2$ given by (32); **b** $|\phi_l(\omega)|^2$ given by (35)

This problem of how to express the EEG potential explicitly in terms of the synaptic firing rates arises (i) from the difficulty of accurately representing the volume conduction of extracellular currents, and (ii) from the fact that the contribution of each ϕ needs to be weighted by a morphological factor, which depends on the number and geometric distribution of synapses of each type on the many different morphological categories of neurons. Cell morphology matters, since spherically symmetric activation of a neuron will produce less current at distant (e.g., scalp) sites than asymmetric activations. Pyramidal neurons are elongated, aligned, and numerous, and so their activation by ϕ_e, ϕ_l, and ϕ_i is likely to be the main contribution to EEGs. Ideally we would like to calculate the power spectrum for some linear combination of these signals, and fit that to experimental data. Unfortunately current physiological knowledge of neuronal interconnections does not allow estimation of the relative contributions of ϕ_e and ϕ_l [ϕ_i is likely to be less important since the proportion of inhibitory connections is known to be small (Liley and Wright 1994)]. In the absence of firm evidence to the contrary, we shall tentatively adopt the values in Table 1, obtained by fitting (33) to the spectrum in Fig. 1a. In particular, they will be used in the following discussion of ERPs.

3.2 Evoked response potentials

The basic equations describing impulse responses of the system depicted in Fig. 2 are (38) and (40). Introducing an impulse into the system, assuming parameters from Table 1, results in the responses in Fig. 4, which are unlike observed ERPs: both $\phi_e(R,t)$ and $\phi_l(R,t)$ show evidence of a damped resonance at the alpha frequency that is superimposed on an upward baseline shift: cf. Fig. 1b.

However, as mentioned in Sect. 2.1 and as described by other authors (Destexhe 2000; Steriade et al. 1990; Swick et al. 1994), there are physiological reasons for expecting thalamic gain modulations after stimuli.

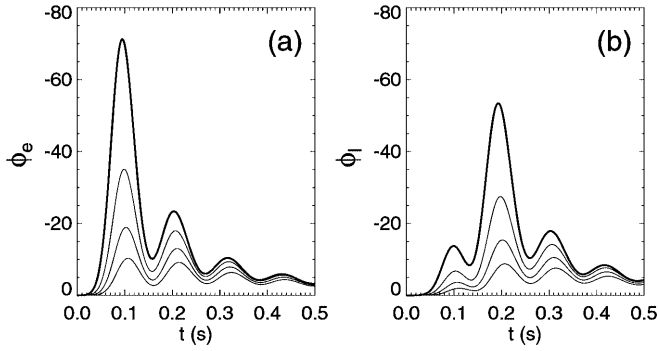

Fig. 4a,b. Firing rates – **a** $\phi_e(R,t)$, and **b** $\phi_1(R,t)$ – for parameters from Table 1, expressed as deviations from the steady state values. The stimulus occurs at $t_{onset} = 0.03$ s and is Gaussian in form, with a temporal standard deviation of 0.02 s and a spatial standard deviation of $r_s = 0.12r_e = 0.01$ m at the cortex. Responses are plotted for four distances from the focus of the stimulus: $R = 0.5r_e$ (*thick line*), r_e, $1.5r_e$, and $2r_e$. Vertical units are arbitrary. Increases in ϕ are shown as negative values, in accordance with the expected changes in scalp potential when $\phi_{e,1}$ acts on the apical dendrites of pyramidal cells, or when ϕ_i acts on the basal dendrites or the cell body

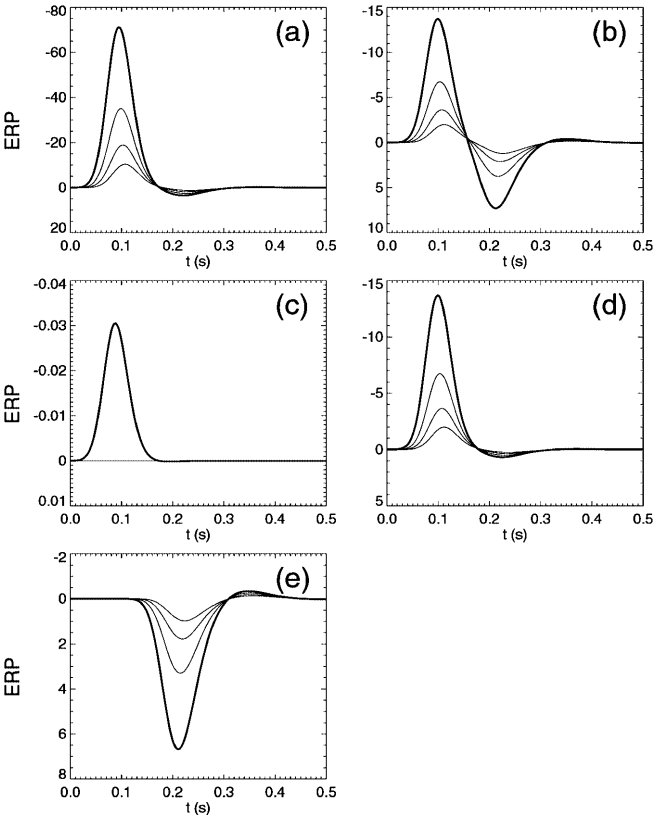

Fig. 5a–e. Responses $\phi_e(R,t)$ **a** and $\phi_1(R,t)$ **b**. The three components of $\phi_1(R,t)$ in (40) are plotted separately as **c**–**e**. Vertical units are arbitrary, and each figure shows responses at four distances from the focus of the stimulus: $R = 0.5r_e$ (*thick line*), r_e, $1.5r_e$, and $2r_e$, as in Fig. 4. Parameters are as in Table 1 and Fig. 4. Note the diminishing size and increasing delay of the peaks as the distance R from the stimulus increases, as expected from the finite axonal conduction speed, $v \approx 10$ m s^{-1}. In **c** all responses are essentially flat except for the case $R = 0.5r_e$

Following the implications of the searchlight hypothesis (Crick 1984), where focal enhancement and general inhibition of cortex is postulated to underlie attention, we shall hypothesize that after a stimulus, relay gains are altered to induce a positive corticothalamic feedback loop of a more focal kind. (The pathways and physiological mechanisms supporting this hypothesis are discussed in Sect. 4.) Specifically, if the positive feedback is so focal that throughout most of the cortex direct corticothalamic (i.e., positive) feedback is suppressed ($G_{es}G_{se} \to 0$), then we find that the impulse responses are as shown in Fig. 5a and b. (It is also assumed that the thalamic modulations take effect at any time prior to the arrival at the thalamus of the impulse response from the cortex; i.e., $\lesssim$100 ms poststimulus.) By comparing Fig. 5a and b with Fig. 4a and b it is apparent that both $\phi_e(R,t)$ and $\phi_1(R,t)$ are affected by these modulations of thalamic gain. Most notable are the elimination of the $\sim$100 ms periodicity and the prolonged upward offset.

The appearance in Fig. 5b of a minimum at $\sim$0.2 s is of particular relevance to ERP modeling. It can be understood by considering the three components of $\phi_1(R,t)$ plotted in Fig. 5c–e, and corresponding to the three terms in (40). Component 1 of $\phi_1(R,t)$ contributes little to the total because it is limited in extent to the stimulated area; component 2 is more widespread and is delayed by cortical propagation; and component 3 is like component 2 except that it is further delayed by the corticothalamic feedback delay and inverted by the negative feedback character of the corticothalamic loop ($G_{es}G_{sr}G_{re} = -0.98$). The contribution of component 1 is further limited by the fact that thalamocortical connections are largely to *spiny stellate* neurons in the sensory cortex, which are not expected to give rise to scalp potentials due to their isotropic dendritic structure. As a result of initial propagating excitation and the delayed negative feedback, $\phi_1(R,t)$ [and to a much lesser extent $\phi_e(R,t)$] have a biphasic appearance like that of a basic ERP, such as in Fig. 1b. Another similarity between the modeled response in Fig. 1b and experimental ERPs is that both typically consist of extrema of similar size and opposite sign. This is not the case for the resonant system implied by Table 1 and demonstrated in Fig. 4, but occurs robustly in this model once thalamic modulation is introduced, as above.

Figure 5 demonstrates the basic character of impulse responses expected from our model. However there are several additional details that will now be considered: (i) the location of the impulse source, (ii) the extent of the area stimulated by the driving signal, and (iii) size of the relative contributions to the observed response from each of the three neuronal populations.

We note that sensory stimuli affect the thalamus broadly: by direct input, via collaterals, and via the brainstem reticular system. Also the N1 ERP component is generated almost simultaneously in the central and secondary auditory cortexes (Näätänen and Picton 1987), suggesting a subcortical source triggered at about the time the sensory stimulus reaches the thalamus. Accordingly, in Fig. 5 and in all subsequent figures, we assume an impulse to be produced within the thalamic

relay nuclei at ~30 ms poststimulus. Regarding the size of the cortical area stimulated by the driving signal, more anatomically detailed modeling of the pathways may help to resolve this uncertainty, but is arguably small due to the fine functional structure of the primary sensory cortex (specifically, $r_s = 10$ mm is assumed). The third matter mentioned above relates to microscopic anatomy, as ϕ_e, ϕ_l, and ϕ_i all contribute to the scalp potential, but with unknown proportions that depend on the number, morphology, and connectivity of the various classes of neurons. Dominance of ϕ_l or ϕ_i is favored by the present evidence since $\phi_e(R,t)$ does not have the required biphasic character of real ERPs. Regarding the relative significance of ϕ_l and ϕ_i, we note that if inhibitory synapses are concentrated near the base of pyramidal cells then they are not as effective at generating current dipoles. Accordingly, in the following figures only $\phi_l(t)$ will be shown.

Although Fig. 5b is a fair approximation to the background ERP shown in Fig. 1b, the N2 and P3 extrem a observed in target ERPs call for additional hypotheses. In generating Fig. 5 we simply assumed that the majority of the cortex is purely under the influence of negative corticothalamic feedback. In the case of target stimuli, however, we propose that the area of cortex subject to thalamic inhibition will not be so extensive since the stimulus is more significant. Such stimuli will require more perceptual and memory resources compared with background stimuli, and so the cortical area needing to be activated (the breadth of the spotlight) will be correspondingly larger. Activation of a greater area of cortex could be achieved by partitioning the cortex and thalamus into two parts: one for which the corticothalamic loop gain is positive (activated), and the remainder for which the loop gain is negative. This is facilitated by the compartmentalization of the thalamus and corticothalamic pathways (Alexander et al. 1990).

In our model, we can approximate background and target responses by supposing that $G_{es}G_{se} \to 0$ following a background stimulus (i.e., little positive feedback), but that this parameter increases according to stimulus significance. Figure 6 shows the result of fits to experimental data when most parameters are held constant, and Table 2 lists the values of the remaining parameters. The inferred values of $G_{es}G_{se}$ support these principles just described. It is notable that the remaining model parameters are largely identical to those obtained separately from a fit of our model to the subjects' average EEG *spectra*. Modulation of $G_{es}G_{sr}G_{re}$ is also expected, since the extent and degree of inhibition is also likely to be a function of stimulus significance. The difference in the value of t_0 is not implied by the above proposals, but nor is it surprising given that several corticothalamic loops have been distinguished on anatomical and functional grounds (Alexander et al. 1990), and that slower loops might be activated in the case of significant stimuli. Note that overall normalization is arbitrary since we have no way of knowing the relationship between firing rates and scalp potential, however it was constrained to be the same for both the ERP fits since we expect the relationship to be constant.

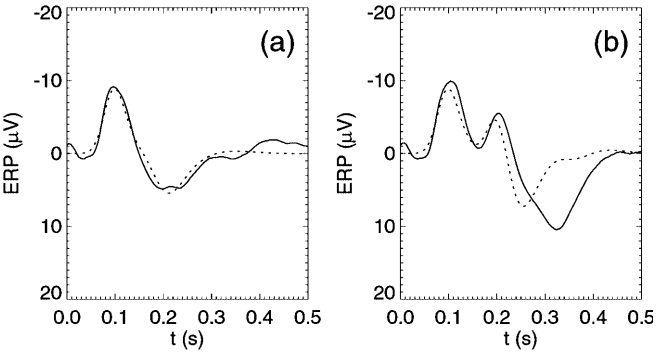

Fig. 6a,b. Fits of $\phi_l(r_e/2,t)$, to the experimental ERPs shown in Fig. 1b: **a** background ERP, **b** target ERP. Experimental ERPs are shown as *solid lines*, fitted ERPs as *dotted lines*. The parameters are as in Table 1, other than $G_{es}G_{se}$, $G_{es}G_{sr}G_{re}$, and t_0. The stimulus was assumed to have the form of a normal distribution with mean of 0.03 s and SD of 0.02 s

Table 2. Thalamic parameters corresponding to the spectral fit in Fig. 1a and ERP fits in Fig. 6. The three fits are distinguished only by the parameters listed here: the remainder are as in Table 1

Parameter	EEG	Background ERP	Target ERP
$G_{es}G_{se}$	6.9	0.0	2.9
$G_{es}G_{sr}G_{re}$	−1.0	−1.0	−3.7
t_0 (s)	0.08	0.08	0.10

The additional upward-going component of the target response, Fig. 6b, which would be labeled 'N2' in ERP literature, can be attributed to the initial cortical signal passing through the *positive* feedback loop from cortex to secondary relay nuclei and back to cortex, with a gain parameterized by $G_{es}G_{se}$. The time difference between the N1 and N2 peaks is closely related to the delay in the corticothalamic loop, t_0. As a result, background ERP is reproduced simply through thalamic gain modulations, and the N1–P2–N2 sequence of peaks in the target ERP is similarly reproduced by our model, although the final P3 peak is distorted. The characteristics of the model will be discussed further in Sect. 4, as will possible reasons for the remaining discrepancies in Fig. 6a and b between the model and experimental ERPs.

4 Discussion

In this paper we have introduced two new structural elements to our previous model – a more realistic representation of the thalamus and an additional population of cortical neurons – and raised the question of the location of the driving signal. Each of these elaborations contributes to the results in Sect. 3.

Looking first at spectral estimates of EEG, many of the consequences of delayed corticothalmic feedback have been explored in a simpler thalamic model by Robinson et al. (2001b). The more detailed effects of the present thalamic representation, as well as questions of the location of the noise source and the relative contri-

butions of the different cortical populations, are found to have relatively minor consequences. These refinements are the subject of current investigation and are not critical to the present ERP results, so they will not be discussed further here.

The effects of neural population (i.e., axon range) and various thalamic gains manifest clearly in impulse responses, which we identify here with ERPs. We see from Fig. 5 that $\phi_e(R,t)$ has a rapidly damped response that is little affected by the corticothalamic feedback. The characteristic time constant r_e/v for cortical propagation is small ($\approx$10 ms), so the response is heavily damped, although this also depends on the gain of the feedback loop. This is in contrast to the case of $\phi_1(R,t)$, for which analytical expressions are naturally represented as multiple components. Thus the first two components of $\phi_1(R,t)$ in (40) are closely related to the initial impulse reaching the cortex, and are nearly coincident. The third component includes the factor $\mathscr{S}$ which is the corticothalamocortical transfer function defined by (8), and allows both for positive and negative corticothalamic feedback with the parameters $G_{es}G_{se}$ and $G_{es}G_{sr}G_{re}$, respectively. These parameters are critical to reproducing ERPs.

Figure 7 demonstrates many of the possible responses of the system in terms of $G_{es}G_{se}$ and $G_{es}G_{sr}G_{re}$. We see that the main effect of $G_{es}G_{se}$, the strength of the positive corticothalamic feedback via secondary thalamic relay nuclei, is to modulate the amplitude of the peak at $\sim$0.2 s. Since the neurons in this path are excitatory, the $\sim$0.2-s peak has the same sign as the $\sim$0.1-s peak, and the separation of these two peaks is approximately t_0 plus the delay $1/\eta_1 + 1/\eta_2$ occurring in the thalamus. The value $G_{es}G_{sr}G_{re}$ quantifies the strength of the alternative corticothalamic pathway. This pathway involves an additional nucleus (the reticular nucleus) consisting of inhibitory neurons, and so results in a trough at a time that is slightly delayed with respect to the $\sim$0.2-s peak.

On the basis of the pattern of results in Fig. 7 we expect the values $G_{es}G_{se} = 6.9$ and $G_{es}G_{sr}G_{re} = -1.0$ from Table 1 to result in multiple periodic maximums in ϕ_1, which is indeed similar to the waveforms in Fig. 4. Based on the seachlight hypothesis, it is proposed that both $G_{es}G_{se}$ and $G_{es}G_{sr}G_{re}$ may be modulated following a stimulus. We find that responses resembling backgrounds occur near the left of Fig. 7 and have P2-like components that can largely be attributed to the negative feedback loop through the reticular nucleus, as shown explicitly in Fig. 5e. In target-like responses – roughly the middle of Fig. 7 – the same minimum is present, but the increased positive feedback causes an N2-like component at about 0.2 s and the emergence of two separate minimums, which are suggestive of the P2 and P3 components of target responses. The responses at the bottom left of Fig. 7 hint at the emergence of a theta-like rhythm for sufficiently strong negative feedback, while a combination of a baseline shift and alpha rhythm occurs for strong positive feedback (upper right). Robinson et al. (2001b) showed, in a delayed corticothalamic feedback model resembling the present one, that spectra are dominated by $\sim$5 Hz when feedback is strongly negative, and by frequencies near zero and $\sim$10 Hz when feedback is strongly positive, in agreement with limiting cases of the present model. They also considered the linear stability of such systems.

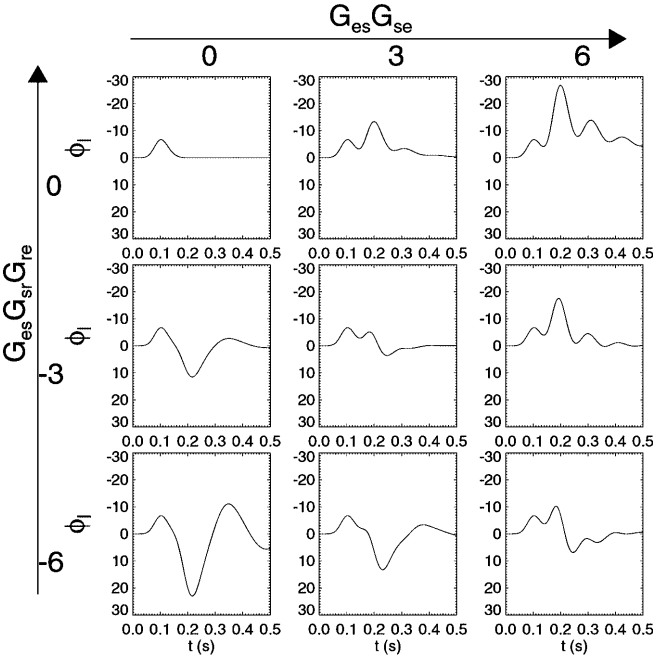

Fig. 7. Responses $\phi_1(t)$ for various values of positive feedback, $G_{es}G_{se} = 0, 3, 6$, and negative feedback, $G_{es}G_{sr}G_{re} = 0, -3, -6$. At the *top left* is the zero feedback case, where only the initial cortical response occurs. Parameters are as in Table 1 and Fig. 4 with $R = 0.5r_e$

In summary, according to this model all ERP components are the result of a single impulse occurring in a system whose spectral characteristics can also be matched with an identical model and largely identical parameters. The main types of response (alpha and theta rhythms, and background and target ERPs) are seen as resulting from modulations of the gains of the relay and reticular nuclei of the thalamus.

Figure 8 shows the effects of variations to individual parameters other than $G_{es}G_{se}$ and $G_{es}G_{sr}G_{re}$. The rate constants γ_e, α, β, η_1, and η_2 generally have little effect on the impulse responses. The cortical gains $G_{ll} + G_{ii}$ and G_{ee} simply scale the response magnitude, and variations in the corticothalamic loop delay t_0 affect the separation of the components. Variations in the stimulus parameters t_{onset}, t_s, and r_s offset the response or alter the shape of the response in ways that do not affect its overall character.

As mentioned in Sect. 3.1, $G_{sr}G_{rs}$ becomes relevant when $G_{sr}G_{rs}$ approaches a critical value. Near this limit (dashed line in Fig. 8l) an unstable resonance occurs between the secondary relay and reticular nuclei, whose properties have been examined in detail by Lopes da Silva and coworkers (e.g., Lopes da Silva 1991). The resonance has a characteristic frequency close to $\sqrt{\eta_1\eta_2} \approx 130\ \mathrm{s}^{-1} \approx 20$ Hz, which is distinct in mechanism and frequency from the alpha and theta rhythms in Fig. 7. The gain $G_{sr}G_{rs}$ is constrained by physiology to

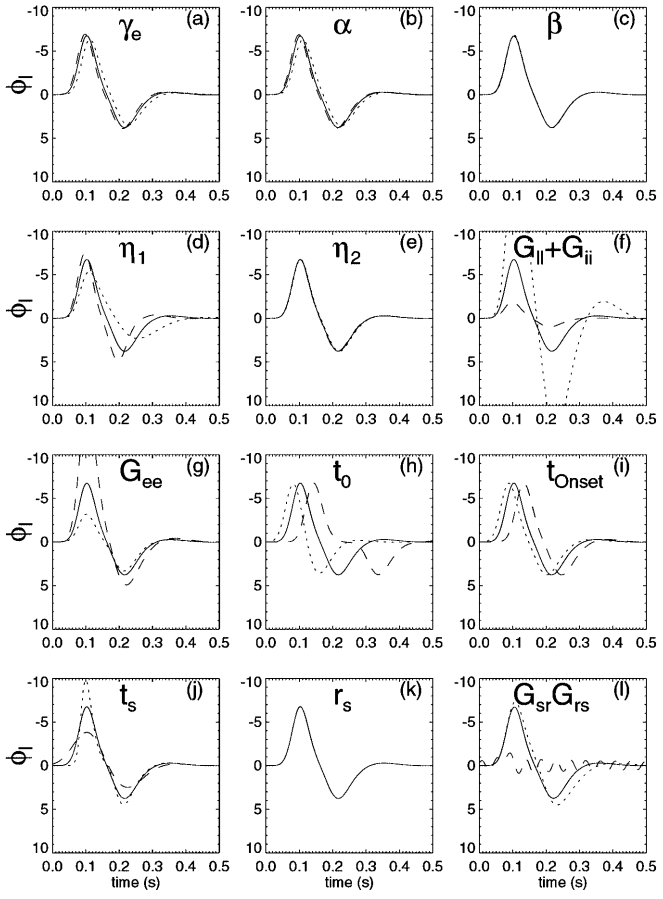

Fig. 8a–l. Effects on $\phi_1(t)$ of variations to parameter values. Each plot is labeled with the parameter being varied. The *solid line* shows $\phi_1(t)$ for the parameters from Table 1 (except $G_{es}G_{se} = 0$, as in Fig. 6), and for the stimulus parameters used in other figures. Variations by a factor of 0.5 are shown as *dotted lines*, while *dashed lines* are for variations by a factor of 2. Panel l is an exception: the response for $G_{sr}G_{rs} = -0.14$ is shown as a *solid line*, while the *dotted line* is for a value of 0 and the *dashed line* is for a value of −10

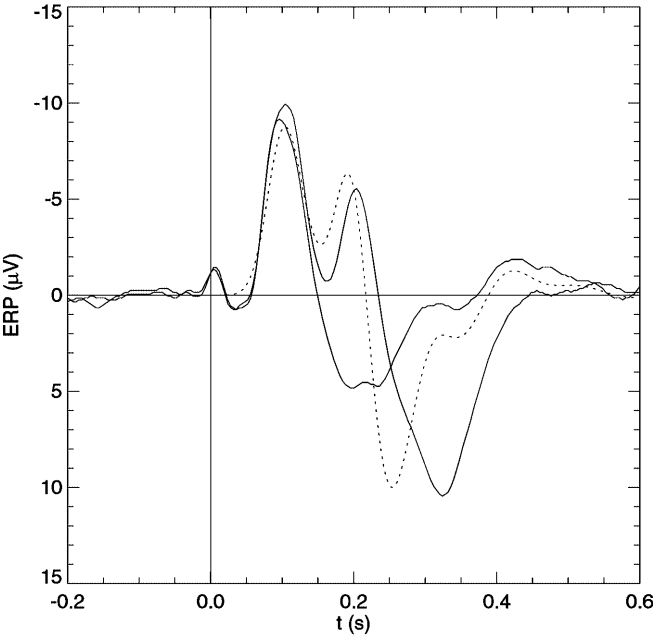

Fig. 9. Experimental background and target ERPs (*solid lines*) and a theoretical ERP with the same parameter values as in Fig. 6b except $G_{es}G_{se} = 4.0$, $G_{es}G_{sr}G_{re} = -5.0$, and $t_0 = 0.09$ s

be negative, so the other limit is a value of zero. At this extreme (dotted line in Fig. 8l) the response has a deepened and prolonged trough, which may used to account for the discrepancy observed in Fig. 6b.

Another possibility for improving the quality of the fits in Fig. 6a and b is suggested by Fig. 9. The parameters of the partially successful fit in Fig. 6b fail to reproduce the depth of the P3 trough, however if the thalamic gains are increased by about 40%, then this failure can be overcome, leaving only the latency difference to overcome. (A model in which target stimuli activate longer and slower corticothalamic feedback loops would have the required effect.) The same strengthening of thalamic gains also results in low amplitude ~10 Hz oscillations near 0.4 s, which may help in fitting the later part of the background response, where a similar oscillation is observed. However these refinements are hard to investigate with our present analytical methods, and call for a numerical approach.

The model deals only with one effective cortico–thalamo–cortical pathway, and identifies separately modulated positive and negative feedback loops as critical to ERP generation. However it is of interest to note the similar proposal by Houk (1995) of a positive feedback loop linking the cortex, basal ganglia, and thalamus, but which assumes a negative feedback character in response to novel situations (cf. our 'target' stimuli). Likewise Kropotov and Etlinger (1999) have independently proposed a similar circuit based on extensive intracerebral recordings. Moreover, the existence of multiple corticosubcortical loops has been pointed out by Alexander et al. (1990). Consequently we see the present results as having relevance beyond the particular case shown in Fig. 2, since they are easily generalized to include loops of these alternative types.

It is difficult to provide a definitive argument for a single specific physiological mechanism for thalamic gain modulation, since there are several modulatory influences acting on the thalamus and cortex. One candidate is noradrenaline from the locus ceruleus, which has long been known to be associated with tonic arousal (Moruzzi and Magoun 1949) and with transient attentional shifts (Pineda et al. 1987). Another is acetylcholine, which is released from the parabrachial region of the brainstem, and constitutes the principal input to the thalamus from the brainstem (Sherman and Koch 1998). Acetylcholine has been shown experimentally and computationally to be the likely cause of the radical changes in the character of the thalamus, where there is modulation of the efficacy of the TRN leading to switching between slow wave and spindle sleep states (Destexhe 2000). The effect of both these metabotropic modulators is to alter the effective gains connecting the thalamic elements, and consequently alter the resonant properties of the system. The phenomenon of alpha blocking might be reflecting these shifts in system parameters. Additional factors contributing to the effective gain

values are the spatial coherence (Destexhe 2000) and temporal synchrony (Sillito et al. 1994) of action potentials.

It is interesting to note that gain modulation has long been invoked in the neuropsychological literature. The searchlight hypothesis is one example; another is the proposal by Pribram and McGuinness (1975) for corticothalamic loops to mediate arousal and activation.

Modulation of gain could also occur as the result of the intensity of firing rate arriving at thalamic nuclei. The present results were obtained by linearizing the neuronal response function (5) so that G_{ab} are all constant over time, but for sufficiently large impulses the static nonlinearity of this function will cause each G_{ab} to become (to a first-order approximation) proportional to the instantaneous average depolarization within the nucleus. These temporal gain modulations are in addition to those due to neuromodulators. It is of interest to note that Jansen and coworkers used this static sigmoidal nonlinearity to model a relationship between prestimulus alpha phase and ERP amplitude (Jansen and Rit 1995; Jansen et al. 1993), and so this mechanism may be an alternative explanation for event-related gain modulations.

5 Conclusion

We have described a new version of our continuum model of the EEG that has a more realistic representation of thalamic anatomy, and reflects the broad classes of cortical neurons more accurately. The continuum approximation permits large-scale dynamics to be modeled, and complements the network style of modeling. As with previous versions of this model, analytical expressions for the expected EEG spectrum could be obtained, which are suitable for parameter estimation through inverse modeling. The spectrum of the long-range excitatory activation field ϕ_e is identical to that from our earlier model, while that of the newly introduced short-range activation field ϕ_1 is qualitatively similar, although it is a weaker function of frequency. When model parameters were obtained from experimental spectral data, and combined with thalamic gain modulations consistent with psychological theories relating to the orienting response, the model was shown to result in impulse responses $\phi_1(t)$ that resemble ERPs. The critical parameters that differed from those obtained from the same subjects' EEGs were gains within the TRN and the thalamic relay nuclei. ERPs resembling typical 'background' responses were obtained whenever corticothalamic feedback became predominantly negative, while 'target' tones could be modeled by retaining some degree of positive feedback. These were argued to be the same changes as those expected from the principles contained in the 'searchlight hypothesis' (Crick 1984). The modeled ERPs satisfy the criteria that the response onsets are correct, the responses are transient rather than being sinusoidal, they have the appropriate sequence of positive- and negative-going sequence of extrema, and the majority of parameters are identical to those obtained from fitting the corresponding model of EEG spectra to experimental data.

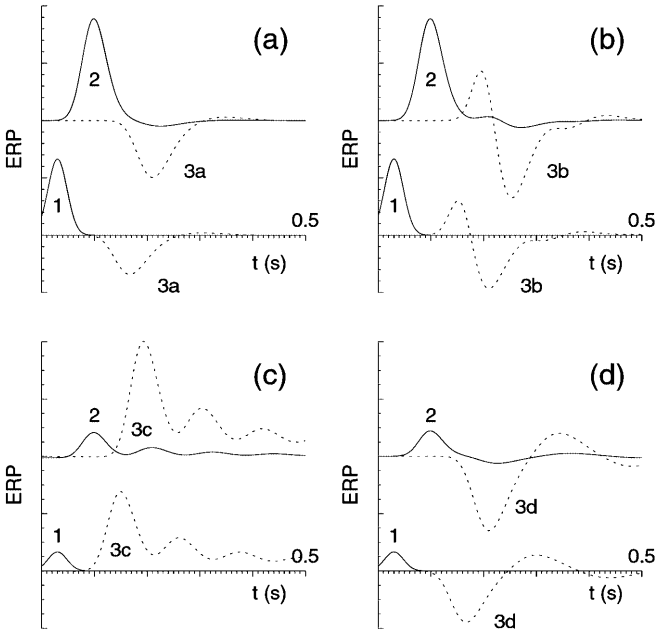

Fig. 10a–d. Evoked potentials (arbitrary units) corresponding to four combinations of positive ($G_{es}G_{se}$) and negative ($G_{es}G_{sr}G_{re}$) corticothalamic feedback strengths, illustrating the four distinct states described in the text: **a** $G_{es}G_{se} \to 0$, and $G_{es}G_{sr}G_{re}$ unchanged from resting value; **b** $G_{es}G_{se} \approx |G_{es}G_{sr}G_{re}|$; **c** $G_{es}G_{se} \gg |G_{es}G_{sr}G_{re}|$; **d** $G_{es}G_{se} \ll |G_{es}G_{sr}G_{re}| >$ resting value. In each case the initial thalamic and cortical responses (*solid lines*) are plotted separately from the responses resulting from corticothalamic feedback (*dotted lines*), and are labeled as in the text. The thalamic responses are plotted below the cortical responses, and so precede the latter by an amount approximately equal to the thalamocortical conduction delay

The proposed sequence of events following a stimulus is as follows (see Fig. 10):

1. An impulse, consisting of the sensory signal and associated activity due to collaterals, arrives at the thalamus 20–30 ms after a stimulus.
2. The thalamic response is relayed to the appropriate part of the cortex, resulting in the first negative (N1) peak. Activation of pyramidal neurons with long axons is propagated through the cortex; activation of locally connected pyramidal neurons is *not* propagated beyond the area of the initial cortical activation. The latter population reinforces the initial cortical excitation, helping to create a synchronized cortical activation, which is in part directed at the thalamus. This second volley to the thalamus reaches it ~100 ms after the first.

3a. By a mechanism probably involving neuromodulators or thalamocortical collaterals, the initial volley to the thalamus also widely suppresses the normal feedback route between the cortex and the thalamic relay nuclei. This alters the transfer characteristics of the thalamus such that the positive feedback is largely removed, while the negative feedback route (via the TRN) remains. The second cortical volley is thus inverted with respect to the N1 component, resulting in the P2 ERP component, and is delayed by ~100 ms.

3b. If the significance of the stimulus requires a greater portion of the relay nuclei to be disinhibited, then the second volley will be a mixture of a positive and negative feedback. The negative feedback component is delayed and broader due to having passed through the TRN, and so the mixed response is asymmetric, resulting in the N2 and P3 ERP components.

3c. States of *nonfocal* attention have positive feedback characteristics ($G_{es}G_{se} \gg |G_{es}G_{sr}G_{re}|$), which are associated with an alpha-like resonance.

3d. States of *focal* attention may have isolated areas with positive corticothalamic feedback, but generally the system will have negative feedback characteristics ($G_{es}G_{se} \ll |G_{es}G_{sr}G_{re}|$), which are associated with a theta-like resonance.

This scheme accounts for ERPs in terms of thalamic gain changes having durations at least as long as that of ERPs, and shows that these gain changes result in impulse responses similar to those observed. It also is compatible with general EEG distinctions between alpha and theta states. Nevertheless, there is a large body of work on the phenomenology of ERPs which has scarcely been addressed in the present work: there are distinctions that can be drawn between different kinds of P3, prolonged negativities, ERPs obtained during sleep, ERP topography, and responses to missing (but expected) stimuli (Näätänen and Picton 1987). To improve the general applicability of this model we need to make explicit how the limbic and neuromodulator systems influence the critical thalamocortical gains identified above. It would also be desirable to incorporate more information about cell morphology and connectivity in order to clarify the extent to which ϕ_e, ϕ_1, and ϕ_i contribute to scalp potentials.

Further refinements to the model will improve the quantitative predictions of both EEG spectra and ERP waveforms, and will be reinforced by performing fits to a range of normal, clinical, and experimental data. But even with the current version we have demonstrated qualitative matches for both EEGs and ERPs using an identical underlying model, and parameters that are physiologically plausible. This encourages us to believe that much of the phenomenology of ERPs might be explained by a simple linear model of wave propagation through the cortex and subcortical structures.

References

Abramowitz M, Stegun IA (eds) (1965) Handbook of mathematical functions. Dover, New York

Alexander GE, Crutcher MD, DeLong MR (1990) Basal ganglia–thalamocortical circuits: Parallel substrates for motor, oculomotor, "prefrontal" and "limbic" functions. In: Uylings HBM, van Eden CG, de Bruin JPC, Feenstra MGP (eds) Progress in brain research, vol 85. Elsevier, Amsterdam, pp 119–146

Bahramali H, Gordon E, Lagopoulos J, Lim CL, Li W, Leslie J, Wright J (1999) The effects of age on late components of the ERP and reaction time. Exp Aging Res 25: 69–80

Crick F (1984) Function of the thalamic reticular nucleus: the searchlight hypothesis. Proc Natl Acad Sci USA 81: 4586–4590

Destexhe A (2000) Modelling corticothalamic feedback and gating of the thalamus by the cerebral cortex. J Physiol (Paris) 94: 391–410

Houk J (1995) Information processing in modular circuits linking basal ganglia and cerebral cortex. In: Houk JC, Davis JL, Beiser DG (eds) Models of information processing in the basal ganglia. MIT Press, Cambridge, Mass., pp 3–9

Jansen BH, Rit VG (1995) Electroencephalogram and visual evoked potential generation in a mathematical model of coupled cortical columns. Biol Cybern 73: 357–366

Jansen BH, Zouridakis G, Brandt ME (1993) A neurophysiologically-based mathematical model of flash visual evoked potentials. Biol Cybern 68: 275–283

Koch C (1999) Biophysics of computation. Oxford University Press, New York

Kropotov JD, Etlinger SC (1999) Selection of actions in the basal ganglia–thalamocortical circuits: review and model. Int J Psychophysiol 31: 197–217

Liley DT, Wright JJ (1994) Intracortical connectivity of pyramidal and stellate cells: estimates of synaptic densities and coupling symmetry. Netw Comput Neural Syst 5: 175–189

Lopes da Silva F (1991) Neural mechanisms underlying brain waves: from neural membranes to networks. Electroencephalogr Clin Neurophysiol 79: 81–93

Lopes da Silva FH, Hoeks A, Smits H, Zetterberg LH (1974) Model of brain rhythmic activity. The alpha-rhythm of the thalamus. Kybernetik 15: 27–37

Makeig S, Westerfield M, Jung T-P, Covington J, Townsend J, Sejnowski TJ, Courchesne E (1999) Functionally independent components of the late positive event-related potential during visual spatial attention. J Neurosci 19: 2665–2680

Moruzzi G, Magoun HW (1949) Brain stem reticular formation and activation of the EEG. Electroencephalogr Clin Neurophysiol 1: 455–473

Näätänen R, Picton T (1987) The N1 wave of the human electric and magnetic response to sound: a review and an analysis of the component structure. Psychophysiology 24: 375–425

Nunez PL (1974) The brain wave equation: A model for the EEG. Math Biosci 21: 279–297

Nunez PL (1995) Neocortical dynamics and human EEG rhythms. Oxford University Press, New York

Pineda JA, Foote SL, Neville HJ (1987) The effects of locus coeruleus lesions on a squirrel monkey late positive component: a preliminary study. Electroencephalogr Clin Neurophysiol Suppl 40: 481–486

Pribram KH, McGuinness D (1975) Arousal, activation, and effort in the control of attention. Psychol Rev 82: 116–149

Regan D (1989) Human brain electrophysiology. Elsevier, New York

Rennie CJ, Robinson PA, Wright JJ (1999) Effects of local feedback on dispersion of electrical waves in the cerebral cortex. Phys Rev E 59: 3320–3329

Robinson DL (1999) The technical, neurological and psychological significance of 'alpha', 'delta' and 'theta' waves confounded in EEG evoked potentials: a study of peak latencies. Clin Neurophysiol 110: 1427–1434

Robinson PA, Rennie CJ, Wright JJ (1997) Propagation and stability of waves of electrical activity in the cerebral cortex. Phys Rev E 56: 826–840

Robinson PA, Wright JJ, Rennie CJ (1998) Synchronous oscillations in the cerbral cortex. Phys Rev E 57: 4578–4588

Robinson PA, Loxley PN, O'Connor SC, Rennie CJ (2001a) Modal analysis of corticothalamic dynamics, electroencephalographic spectra, and evoked potentials. Phys Rev E 63: 041909

Robinson PA, Rennie CJ, Wright JJ, Bahramali H, Gordon E, Rowe DL (2001b) Prediction of electroencephalographic spectra from neurophysiology. Phys Rev E 63: 021903

Samar VJ, Swartz KP, Raghuveer MR (1995) Multiresolution analysis of event-related potentials by wavelet decomposition. Brain Cogn 27: 398–438

Sherman SM, Koch C (1998) Thalamus. In: Shepherd GM (ed) Synaptic organization of the brain, 4th edn Oxford University Press, New York, pp 289–311

Shibasaki H, Nakamura M, Nishida S (1987) Scalp topography of photic evoked potentials. Applications of wave form decomposition technique. Electroencephalogr Clin Neurophysiol 66: 200–204

Sillito AM, Jones HE, Gerstein GL, West DC (1994) Feature-linked synchronization of thalamic relay cell firing induced by feedback from the visual cortex. Nature 369: 479–482

Steriade M, Gloor P, Llinas RR, Lopes da Silva FH, Mesulam MM (1990) Report of IFCN committee on basic mechanisms. Basic mechanisms of cerebral rhythmic activities. Electroencephalogr Clin Neurophysiol 76: 481–508

Swick D, Pineda JA, Schacher S, Foote SL (1994) Locus coeruleus neuronal activity in awake monkeys: relationship to auditory P300-like potentials and spontaneous EEG. Exp Brain Res 101: 86–92

Wilson HR, Cowan JD (1973) A mathematical theory of the functional dynamics of cortical and thalamic nervous tissue. Kybernetik 13: 55–80

Wright JJ (1999) Simulation of EEG: dynamic changes in synaptic efficacy, cerebral rhythms, and dissipative and generative activity in cortex. Biol Cybern 81: 131–147

Wright JJ, Liley DTJ (1994) A millimetric-scale simulation of electrocortical wave dynamics based on anatomical estimates of cortical synaptic density. Netw Comput Neural Syst 5: 191–202

Wright JJ, Sergejew AA, Stampfer HG (1990) Inverse filter computation of the neural impulse giving rise to the auditory evoked potential. Brain Topogr 2: 293–302

Yingling CD, Skinner JE (1977) Gating of thalamic input to cerebral cortex by nucleus reticularis thalami. In: Desmedt JE (ed) Attention, voluntary contraction, and event-related cerebral potentials (Progress in clinical neurophysiology, vol 1): Karger, Basel, pp 70–96